Coordinated Control for Low Voltage Ride Through in PMSG Wind Turbines

Phuong T.H. Nguyen * **S. Stüdli** * **J. H. Braslavsky** *,** **and R. H. Middleton** *

* *School of Electrical Engineering and Computing, The University of Newcastle, Australia. Email: thihuyenphuong.nguyen@uon.edu.au, {sonja.stuedli, richard.middleton}@newcastle.edu.au*
** *CSIRO Energy, Australia. Email: julio.braslavsky@csiro.au*

Abstract: This work proposes a control strategy for permanent magnet synchronous generator (PMSG) based wind energy conversion systems (WECSs) to improve low voltage ride through (LVRT) capabilities. The nonlinear relationship between the generator speed and DC-link voltage is considered by using feedback linearisation. To support the grid during LVRT, the DC-link voltage is controlled by the machine side converter (MSC). The kinetic energy stored in the wind turbine inertia is used to compensate for lower voltage. Further, pitch angle control is used to ensure stable operation, and to guarantee the rotor speed does not exceed the rated value. A simulation of a 2MW PMSG wind turbine is conducted to validate the proposed control strategy.

Keywords: Permanent magnet synchronous generator, DC-link voltage, low voltage ride through, feedback linerisation, wind energy conversion system.

1. INTRODUCTION

In recent decades, the penetration of wind energy into power systems increased rapidly. Permanent magnet synchronous generator (PMSG) wind turbines are viewed as a promising solution for modern wind energy conversion systems (WECSs) (Haraguchi et al., 2009). A direct drive PMSG is totally decoupled from the grid via a full scale converter, which insulates impacts from network disturbances and provides a large operating speed range (Haraguchi et al., 2009; Muyeen et al., 2010).

Current grid codes demand that wind turbines stay connected to the grid during some disturbances, in particular if the grid voltage drops. This low voltage ride through is a major concern in wind turbine systems (Australian Energy Market Operator, 2011). In this context grid codes define suitable voltage limit curves that guide the disconnection of wind turbines. These curves are illustrated in Fig. 1. Connection must be maintained as long as the grid voltage remains above Limit line 1 and has to disconnect if the voltage is below Limit line 2.

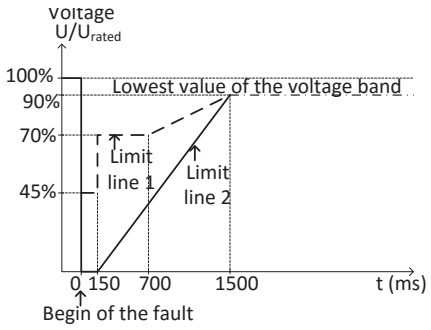

Fig. 1. Voltage limit curves to allow wind turbines disconnection (Mohseni and Islam, 2012).

In addition, to assist grid voltage recovery, wind turbines are required to deliver reactive power to the grid. The amount of reactive current can be calculated from voltage drop curves as shown in Fig. 2 (Mohseni and Islam, 2012; Tsili and Papathanassiou, 2009). That means the active and reactive powers are required to change according to the voltage-time profile and reactive current-voltage profile.

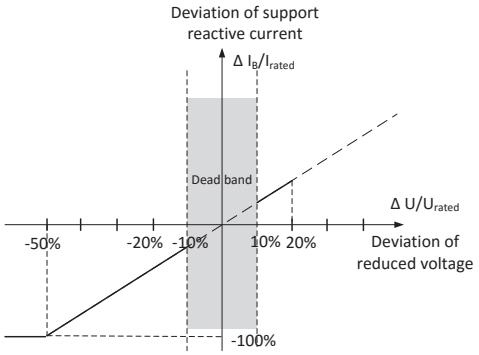

Fig. 2. Reactive current to be injected into the grid during LVRT (Mohseni and Islam, 2012).

During voltage dips, The PMSG will continue supplying active power to the DC-link. The accumulated active power in the DC-link capacitor causes the DC-link voltage to increase. As a result, the DC-link capacitor might be damaged. The traditional solution to limit the increase of the DC-link voltage is to utilize a braking chopper resistance in the DC-link (Abdelrahem and Kennel, 2016; Conroy and Watson, 2007; Geng et al., 2011), to dissipate redundant active power. However, this solution can only dissipate the surplus power and cannot deliver reactive power to the grid. To improve the performance of wind turbines during grid faults, the work of Muyeen et al. (2010) addressed

LVRT issues by using a flexible alternating current transmission system to deliver reactive power although at an additional system cost. Storing excess power in the DC-link is another option. An energy storage system for WECS is proposed by Xu et al. (2013), although also substantially adding to system costs.

Conventionally, the machine side converter (MSC) controls the power generated from the wind turbine by controlling the rotor speed while the grid side converter (GSC) controls the DC-link voltage to balance the input and output powers. In a strong grid, wind energy is a relatively small portion of the power system, such that the GSC can regulate the DC-link voltage to achieve the desired power transfer from the generator to the grid (Conroy and Watson, 2007; Uehara et al., 2011; Yuan and Li, 2014). However, this strategy is impractical when the GSC needs to regulate grid-side voltage and frequency, while the DC-link voltage should be more naturally controlled by the MSC. In such case, the natural variability in wind resource and the nonlinearities of wind power conversion make hard for the conventional control strategy to maintain the DC-link voltage within an appropriate range (Yuan et al., 2009).

Some studies address this problem by introducing a PI controller for the MSC to govern the DC-link voltage (Geng et al., 2011; Hansen and Michalke, 2009). This control is complicated due to the nonlinear relationship between DC-link voltage and rotor speed. To address nonlinearities, hybrid adaptive control approaches have been proposed (Yuan and Li, 2014; Yuan et al., 2009), as well as fuzzy-logic control (Yassin et al., 2016) and feedback linearisation (Kim et al., 2012; Van et al., 2015). These DC-voltage strategies, however, do not include reactive power support for LVRT. Moreover, they do not guarantee that during faults the wind turbine speed or DC-link voltage are held within their constraints.

This paper considers the nonlinear relationship between the generator speed and the DC-link voltage by using a feedback linearisation technique to improve the performance of PMSG wind turbines for LVRT without need for expensive additional hardware components. In the proposed approach, the electrical power of the PMSG is controlled according to the grid connected power of the GSC and the wind turbine inertia is employed to store the excess power. Reactive power is also delivered to support grid voltage recovery in compliance with the current grid code requirements. Simulation results illustrate the effectiveness of the proposed strategy as compared with a strategy based on a conventional PI controller.

2. MODELLING OF THE PMSG-BASED WECS

The general model of a PMSG-based WECS is shown in Fig. 3.

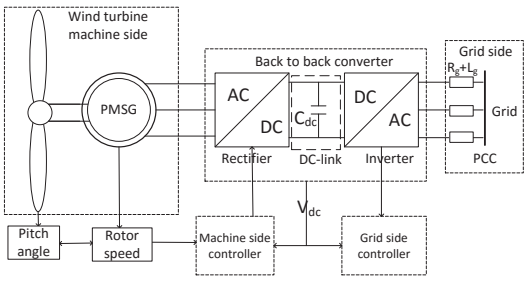

Fig. 3. The general model of a PMSG-based WECS

2.1 Wind turbine model

The wind power, P_w, can be computed as $P_w = \frac{1}{2}\rho A V_w^3$, where: ρ is the air density $[kg/m^3]$, A is the area swept by the wind turbine's blades $[m^2]$ and V_w is the wind speed $[m/s]$. The actual mechanical power P_m extracted from the wind power is proportional to the coefficient of performance C_p, i.e., $P_m = C_p P_w = C_p\left(\frac{1}{2}\rho A V_w^3\right)$. C_p can be expressed as a function of λ, tip-speed ratio, and β, pitch angle, i.e.(Heier, 2014),

$$C_p = 0.5176\left(\frac{116}{\lambda_i} - 0.4\beta - 5\right)e^{\frac{-21}{\lambda_i}} + 0.0068\lambda, \qquad (1)$$

where λ and λ_i are defined by

$$\frac{1}{\lambda_i} = \frac{1}{\lambda + 0.08\beta} - \frac{0.035}{1+\beta^3} \qquad \text{and} \quad \lambda = \frac{R\omega_{wt}}{V_w},$$

where R is the radius of the rotating turbine blade $[m]$, and ω_{wt} is the angular speed of the turbine $[rad/s]$. The mechanical torque can be expressed as $T_m = P_m/\omega_{wt}[N.m]$.

2.2 Drive train model

When focusing on decoupling a variable-speed wind turbine from the grid using fully-rated power electronic converters, the drive train can be treated as a one-mass lumped model with acceptable precision (Hamatwi et al., 2016). The turbine electromagnetic torque can then be expressed as

$$J\frac{d\omega_r}{dt} = T_m - T_e - B\omega_r, \qquad (2)$$

where J is the combined inertia, B is the damping coefficient of the turbine, T_e is the electromagnetic torque of the generator, ω_r is the rotor speed of the wind turbine given as $\omega_r = \omega_{wt}$, assuming there is no gearbox.

2.3 Permanent magnet synchronous generator model

The inverse Park and Clarke transforms are introduced to model the three phase AC output from the generator model (Grenier and Louis, 1995). The dynamic model of a PMSG can be expressed by an equivalent circuit in the direct and quadrature axis frame (d,q-axes) (Kundur, 1994) given as

$$v_{ds} = -i_{ds}R_s - \omega_e\lambda_{qs} + \frac{d\lambda_{ds}}{dt}, \qquad (3)$$

$$v_{qs} = -i_{qs}R_s + \omega_e\lambda_{ds} + \frac{d\lambda_{qs}}{dt}, \qquad (4)$$

where i_{ds} and i_{qs} are the stator currents, respectively $[A]$, v_{ds} and v_{qs} are the stator voltages $[V]$, λ_{ds} and λ_{qs} are the stator flux linkages $[Wb]$ all in the d-axis and q-axis respectively, R_s is the resistance of the stator $[\Omega]$, ω_e is the angular electrical rotating speed of the generator $[rad/s]$ with $\omega_e = \frac{p\omega_r}{2}$, p is the number of poles of the PMSG.

The d- and q-axis stator flux linkages are related to the d- and q- axis currents by,

$$\begin{aligned}\lambda_{ds} &= -L_{ds}i_{ds} + \lambda_m,\\ \lambda_{qs} &= -L_{qs}i_{qs},\end{aligned} \qquad (5)$$

where λ_m is the permanent magnet flux linkage, L_{ds} and L_{qs} are the stator inductances in the d-axis and q-axis respectively $[H]$.

When the stator d- and q- axis flux linkages are substituted into the voltage (3) and (4), we have,

$$v_{ds} = -i_{ds}R_s + \omega_e L_{qs} i_{qs} - L_{ds}\frac{di_{ds}}{dt}, \tag{6}$$

$$v_{qs} = -i_{qs}R_s - \omega_e L_{ds} i_{ds} + \omega_e \lambda_m - L_{qs}\frac{di_{qs}}{dt}. \tag{7}$$

The electromagnetic torque, T_e, is given by,

$$T_e = \frac{3}{2}\frac{p}{2}\left(\lambda_m i_{qs} + (L_{qs} - L_{ds})\, i_{ds} i_{qs}\right). \tag{8}$$

For a non-salient pole PMSG, $L_{ds} = L_{qs}$, hence the electromagnetic torque can be simplified to $T_e = 3p/4\lambda_m i_{qs}$.

2.4 The back-to-back converter model

Two-level pulse-width modulated voltage-source converters are used to allow bi-directional power transfer between the DC-link and the point of common coupling (PCC). The DC-link provides an energy buffer between the MSC and GSC, allowing for separate control of the converters on the two sides. The model of the back-to-back converter includes a rectifier on the machine side and an inverter on the grid side. These are connected by a DC-link as shown in Fig. 3.

The rectifier model: The rectifier connects the wind turbine generator with the DC-link and is shown schematically in Fig. 4. The mathematical model of the rectifier is given by,

$$\begin{bmatrix} v_{sa} \\ v_{sb} \\ v_{sc} \end{bmatrix} = \frac{1}{3}\begin{bmatrix} 2 & -1 & -1 \\ -1 & 2 & -1 \\ -1 & -1 & 2 \end{bmatrix}\begin{bmatrix} S_a \\ S_b \\ S_c \end{bmatrix} V_{dc}, \tag{9}$$

where v_{sa}, v_{sb}, v_{sc} are the stator voltages of phases a, b and c, S_a, S_b, S_c are the switching states of phase a, b and c, $S_k (k = a,b,c)$ is defined as

$$S_k = \begin{cases} 1 & \text{Upper switch conducts, lower switch blocks,} \\ 0 & \text{Upper switch blocks, lower switch conducts.} \end{cases}$$

T_1, T_3, T_5 are the upper switches, and T_4, T_6, T_2 are the lower switches corresponding to phase a, b and c.

Three phase stator voltages in the *abc* frame can be transformed into the rotating $dq-$axis frame by

$$\begin{bmatrix} v_{sa} \\ v_{sb} \\ v_{sc} \end{bmatrix} = \begin{bmatrix} \cos\theta & -\sin\theta & 1 \\ \cos\left(\theta - \frac{2\pi}{3}\right) & -\sin\left(\theta - \frac{2\pi}{3}\right) & 1 \\ \cos\left(\theta + \frac{2\pi}{3}\right) & -\sin\left(\theta + \frac{2\pi}{3}\right) & 1 \end{bmatrix}\begin{bmatrix} v_{ds} \\ v_{qs} \\ v_0 \end{bmatrix}, \tag{10}$$

where v_0 is the zero sequence voltage.

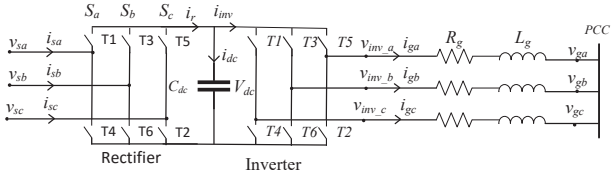

Fig. 4. Model of the machine side rectifier and grid side inverter

DC-link: The relationship between current flow through the DC-link capacitor C_{dc} and the DC-link voltage V_{dc} is given by,

$$C_{dc}\frac{dV_{dc}}{dt} = i_r - i_{inv}, \tag{11}$$

where i_r is the DC output current of the rectifier and i_{inv} is the DC input current to the inverter.

The output current of the rectifier in terms of the switching states is $i_r = i_{sa}S_a + i_{sb}S_b + i_{sc}S_c$.

The inverter model: The wind turbine generator is grid-tied through the inverter as shown in Fig. 4. The three-phase outputs of the inverter are connected to the grid at the PCC via a filter consisting of resistors R_g and inductors L_g. The mathematical model of the GSC can be expressed as

$$L_g\frac{di_{ga}}{dt} = v_{inv\_a} - R_g i_{ga} - v_{ga}, \tag{12}$$

$$L_g\frac{di_{gb}}{dt} = v_{inv\_b} - R_g i_{gb} - v_{gb}, \tag{13}$$

$$L_g\frac{di_{gc}}{dt} = v_{inv\_c} - R_g i_{gc} - v_{gc}, \tag{14}$$

where v_{inv_a}, v_{inv_b} and v_{inv_c} are the output voltages of the inverter, v_{ga}, v_{gb} and v_{gc} are the grid bus voltages, i_{ga}, i_{gb} and i_{gc} are the output currents of the inverter for phases a, b and c.

These equations can be transformed from the stationary *abc* frame into the rotating reference d,q frame as

$$L_g\frac{di_{gd}}{dt} = v_{inv\_d} - R_g i_{gd} + \omega_g L_g i_{gq} - v_{gd}, \tag{15}$$

$$L_g\frac{di_{gq}}{dt} = v_{inv\_q} - R_g i_{gq} - \omega_g L_g i_{gd} - v_{gq}, \tag{16}$$

where v_{inv_d}, v_{inv_q} are the d- and q-axis output voltages of the inverter, i_{gd}, i_{gq} are the d,q-axis output currents of the inverter.

Similarly, the output voltages of the inverter are also related to the switching state of the inverter and the DC-link voltage and the output voltage v_{inv_a}, v_{inv_b} and v_{inv_c} can be transformed into v_{inv_d} and v_{inv_q}.

3. PROPOSED FEEDBACK LINEARISATION CONTROL STRATEGY

3.1 Control of back-to-back converter system

Fig. 5 presents the proposed control scheme for the variable speed PMSG wind turbine based WECS. When there is a voltage dip in the grid side, a reduction of the delivered active power from the DC-link to the grid by the inverter follows. Consequently, the DC-link voltage increases due to the generated active power accumulating in the DC-link capacitor. That might cause damage to the DC-link capacitor.

During a voltage dip, the active power generated from the PMSG wind turbine will decrease according to the percentage of the voltage dip. Consequently, the surplus active power will be stored in the inertia of the rotor of the WECS by increasing the rotor speed. This stored active power will be injected back to the grid after the voltage at the PCC is recovered. In case of LVRT, grid codes require wind turbines to supply reactive power as well. To fulfill this requirement, reactive current will be injected to the grid.

The above process is governed by a cascaded control strategy both for the control of the MSC and the GSC. PI controllers are used in the inner control loops. These have been widely used in many industrial processes because of their simplicity and ease of implementation. However, the nonlinear characteristic of the power generator from the wind turbine limits their performance. Hence, feedback linearisation is utilised for the outer control loop of the MSC. This controller regulates the DC-link voltage, which is controlled at a constant value to regulate the power transferring from the wind turbine generator to the grid. A part of the mechanical power extracted from the wind power will be stored in the wind turbine's rotating mass

when its rotor speed increases or released into the generated power P_g. In the DC-link, the power P_{dc} will be stored in the capacitor and the power injected into the grid will be P_{grid}.

The dynamic equations of the rotor speed and the DC-link voltage (2),(11) can be expressed in terms of power as:

$$\frac{dw_r}{dt} = \frac{P_m}{J\omega_r} - \frac{P_g}{J\omega_r} - \frac{B\omega_r}{J}, \tag{17}$$

$$\frac{dV_{dc}}{dt} = \frac{Pg}{V_{dc}C_{dc}} - \frac{P_{grid}}{V_{dc}C_{dc}}. \tag{18}$$

The output of the system is, $y = V_{dc}$. Hence, the derivative of the output is obtained as

$$\dot{y} = \dot{V}_{dc} = -\frac{P_{grid}}{V_{dc}C_{dc}} + \frac{P_g}{V_{dc}C_{dc}}.$$

The input-output feedback linearisation has been proposed in (Kim et al., 2012). With the control input law $P_g = V_{dc}C_{dc}\left[\frac{P_{grid}}{V_{dc}C}{}_{dc} + v\right]$, we introduce v being the new control law. Then, the derivative of the output is expressed in terms of the new control law as

$$\dot{V}_{dc} = v. \tag{19}$$

The controller is designed to eliminate the tracking error $e = V_{dc} - V_{dc}^{ref}$. Hence, a standard PI control law is used, i.e.

$$v = \dot{V}_{dc}^{ref} - K_1 e - K_2 \int e dt. \tag{20}$$

Using the given relations we find the following equation

$$\dot{V}_{dc} = \dot{V}_{dc}^{ref} - K_1 e - K_2 \int e dt. \tag{21}$$

Rewriting (21), we have:

$$\dot{e} + K_1 e + K_2 \int e dt = 0. \tag{22}$$

From Equation (22), the dynamics of the error in V_{dc} are

$$\ddot{e} + K_1 \dot{e} + K_2 e = 0. \tag{23}$$

Then, the characteristic equation is $s^2 + K_1 s + K_2 = 0$. To achieve asymptotic tracking for the reference value of V_{dc}, the desired poles are designed to be in the left-half plane and we can obtain the values for the gains K_1 and K_2.

The actual control signal for the DC-link voltage control is,

$$u = P_g = P_{grid} + V_{dc}C_{dc}v. \tag{24}$$

The DC-link voltage controller is the outer loop in a cascade controller, with the inner loop controller being the q- axis current controller. The d- and q- axis current controllers are designed by using a vector control strategy with field oriented control. In this strategy, the electromagnetic torque is controlled through the q-axis stator current and the d-axis stator current is set to be zero to maximise generator efficiency.

In the grid side controller, there is a dual-loop control structure based on PI control for d- and q-axes currents with voltage oriented control strategy. By controlling the d- and q- axis currents, the reactive and active powers injected into the grid are controlled respectively. In normal operation, maximum power point tracking (MPPT) can be implemented via the grid side controller based on the tip speed ratio method. In this case, an active power reference value, P_{grid}^* is calculated from the optimal rotor speed ω_{opt} by using the power curve of the wind turbine, while the reactive power reference value is set to zero.

During the fault, the grid side controller is adapted. The active power reference P_{grid}^* is set to zero. Also, in order to support LVRT, a reactive power will be injected into the grid to assist the voltage recovery. The reactive current reference can be calculated from the grid code requirements as

$$I_{gq\_ref} = \begin{cases} 2\left(1 - V_g/V_{g\_rated}\right) I_{rated}, & \text{if } 0.5 \le V_g/V_{g\_rated} \le 0.9 \\ I_{rated}, & \text{if } V_g/V_{g\_rated} \le 0.5 \end{cases} \tag{25}$$

where V_g is the grid voltage magnitude at the PCC and V_{g_rated} is the rated grid voltage.

3.2 Pitch angle control

As discussed in Section 2, the pitch angle affects the performance coefficient C_p. When the pitch angle increases, C_p will decrease. As a result, the mechanical power extracted from the wind power will be reduced. Therefore, the pitch angle is used to control the power from the wind turbine when wind speeds or the turbine rotor speed exceed their rated values. Fig. 6 depicts the pitch angle control scheme. The measured rotor speed of the wind turbine is compared with the reference speed i.e., $1.2\omega_{r\_rated}$. The controller regulates the rotor speed ω_r during a voltage sag. In order to reduce active power generated from the wind turbine, the rotor speed increases and if it is higher than the reference speed, the controller will activate the pitch angle to limit the generated power and reduce the rotor speed.

3.3 Chopper control

The DC-link voltage should remain above V_{dcmin} and below V_{dcmax} to avoid damage. Where V_{dcmin} should meet the grid-side AC voltage amplitude requirement, i.e., $V_{dcmin}M_{max} > \sqrt{2}V_{line}$, where M_{max} is the maximum modulation index of the converter, V_{line} is the line grid voltage magnitude, and V_{dcmax} cannot exceed the voltage ratings of the converter and the DC-link capacitor (Yuan et al., 2009). Hence, a damping resistor is installed in the DC-link of the back-to-back converter as shown in Fig. 5. During a grid voltage drop, if the DC-link voltage is larger than the reference value by 5%, the excess active power will be dissipated by this resistor.

4. SIMULATION RESULTS

Simulations are conducted using a PMSG-based WECSs with 2MW rated power. The parameters of the PMSG wind turbine generator are provided in Table 1 (Bradbury, 2017), and controller parameters are described in Table 2.

Table 1. The wind turbine and PMSG parameters

Wind turbine		Generator	
Cut-in wind speed	4 m/s	Rated power	2MW
Rated wind speed	12 m/s	Rated voltage	690V
Cut-out wind speed	25 m/s	Rated rotor speed	22.5 rmp
Damping coefficient	$1.89.10^{-4}$Nm.s	Stator resistance	0.008556Ω
Blade radius	45 m	Stator inductance	0.00359 H

We will demonstrate the PMSG wind turbine performances with the proposed control strategy for LVRT. The DC-link voltage is controlled in the MSC with consideration of the nonlinear relation between the wind turbine rotor speed and the power generated from the wind turbine. Specifically, the employment of feedback linearisation coordinates with the

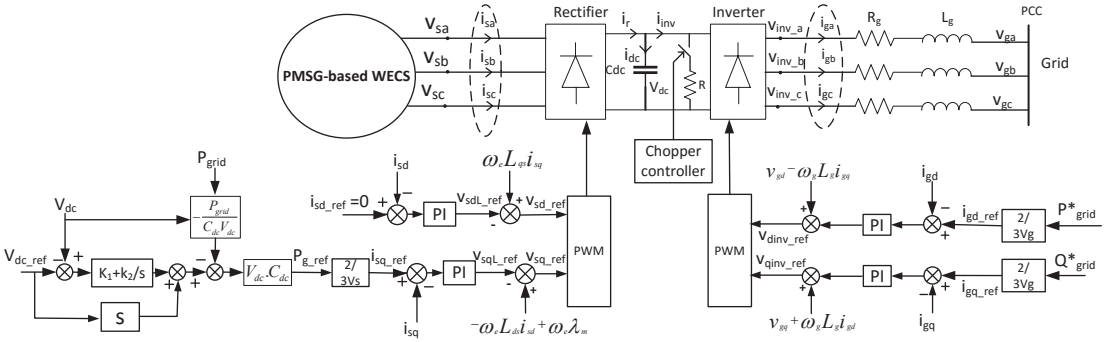

Fig. 5. Feedback linearisation control scheme

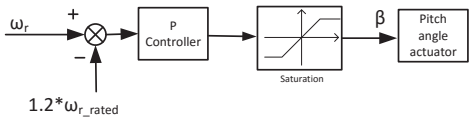

Fig. 6. Wind turbine pitch angle controller

Table 2. Controller parameters

	PI strategy	FLC strategy
V_{dc} controller	$K_i = 16.735$ $K_p = 2.366$	$K_i = 150$ $K_p = 15$
d-axis stator current controller	$K_i = 35.9$ $K_p = 0.5$	$K_i = 897.5$ $K_p = 8.966$
q-axis stator current controller	$K_i = 35.9$ $K_p = 0.5$	$K_i = 897.5$ $K_p = 8.966$
d-axis grid current controller	$K_i = 11.25$ $K_p = 0.076$	$K_i = 20$ $K_p = 0.1114$
q-axis grid current controller	$K_i = 11.25$ $K_p = 0.076$	$K_i = 20$ $K_p = 0.1114$

pitch angle control and reactive power support for grid voltage recovery. Then the simulation is compared with the case when using a conventional PI control strategy to control the DC-link voltage with the MSC.

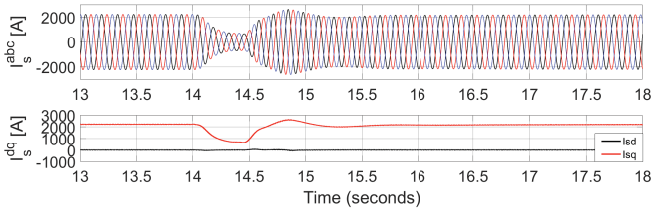

Fig. 7. Stator currents in *abc* frame, and in d- and q-axes with PI control.

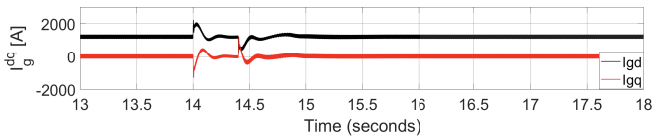

Fig. 8. d- and q-axes grid currents during voltage drop with the PI control.

Simulations of the PI control strategy illustrate the performance of the MSC during a three-phase fault at a wind speed of 8 m/s. At time $t = 14s$, the voltage at the PCC drops by 50%. The active power injected into the grid will decrease during the voltage drop as shown in Fig. 12. Since the DC-link voltage is controlled in the machine side, the rotor speed increases to reduce the power generated from the wind turbine, Fig. 11. Hence, the q-axis stator current decreases as we can see in Fig. 7. Fig. 8 shows the response of d- and q-axes grid currents where the d-axis current does not change much, however the power injected into the grid P_{grid} reduces due to the grid voltage sags, and the q-axis current also remains constant. As a result, there is no reactive power support for grid voltage recovery. Nevertheless, the surplus is still high and the DC-link voltage exceeds 5% of the reference value. Moreover, this control strategy does not provide reactive power support, as required by current grid codes.

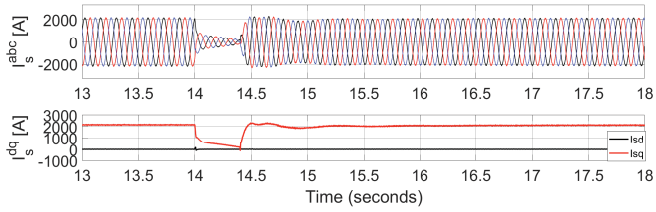

Fig. 9. Stator currents in *abc* frame, and in d- and q-axes with FLC strategy.

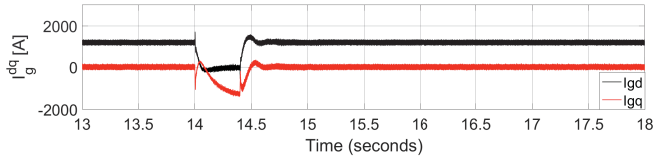

Fig. 10. d- and q-axes grid currents during voltage drop with the FLC strategy.

The performance of the proposed control strategy during the same voltage drop is illustrated in Fig. 9 to 12. As we can see in Fig. 11, when the voltage drop occurs, the MSC controller causes the rotor speed to increase, hence the surplus power is stored in the wind turbine inertia. Compared to the PI control strategy, the rotor speed increase is higher and thus, the generated power decrease lower since the amount of power stored in the wind turbine inertia is larger. Consequently, since the active power transferring through the DC-link decreases, the DC-link voltage will increase less. Fig. 9 shows the d- and q-axes stator currents. Since the q-axis stator current decreases, the active power generated from the wind turbine reduces more significantly than that of the PI control strategy case, the electrical

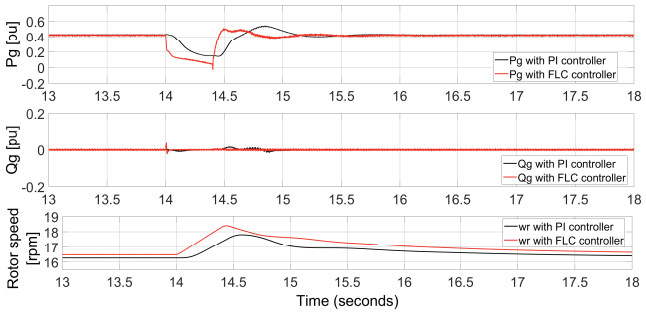

Fig. 11. The active and reactive power generated from the wind turbine generator during the voltage drop with the PI and the proposed control strategies.

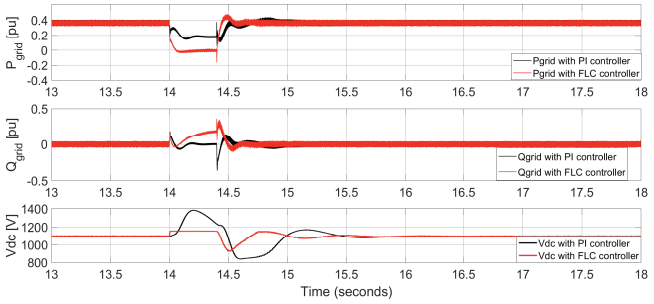

Fig. 12. The active and reactive power injected into the grid, and DC-link voltage during the voltage drop with the PI and the proposed control strategies.

torque also decreases and affects the wind turbine rotor speed increases.

On the GSC, the d- and q-axes grid currents are depicted in Fig. 10. Since the d-axis grid current decreases, the grid active power reduces against the grid voltage reduction. The q-axis grid current decreases to inject reactive power to support grid voltage recovery as illustrated in Fig. 12. As a result, the DC-link voltage is kept below the maximum value limit.

5. CONCLUSIONS

This paper proposed a control strategy for PMSG-based WECS to enhance LVRT capabilities based on the coordination of wind turbine inertia and pitch angle. The simulations show the proposed control strategy improves performance during voltage disturbances as compared to a standard PI control strategy. The proposed control strategy maintains the DC-link voltage within a desired limit range and injects reactive power according to the requirement to support for grid voltage recovery without resorting to additional expensive hardware.

REFERENCES

Abdelrahem, M. and Kennel, R. (2016). Fault-ride through strategy for permanent-magnet synchronous generators in variable-speed wind turbines. *Energies*, 9(12), 1066.

Australian Energy Market Operator (2011). Wind integration: International experience WP2: Review of grid codes.

Bradbury, L. (2017). Wind power and UK wind speed database programs. `http://www.wind-power-program.com/`. Accessed: 2017-09-30.

Conroy, J. and Watson, R. (2007). Low-voltage ride-through of a full converter wind turbine with permanent magnet generator. *IET Renewable Power Generation*, 1(3), 182–189.

Geng, H., Yang, G., Xu, D., and Wu, B. (2011). Unified power control for PMSG-based WECS operating under different grid conditions. *IEEE Transactions on Energy Conversion*, 26(3), 822–830.

Grenier, D. and Louis, J. (1995). Modeling for control of non-sinewave permanent-magnet synchronous drives by extending Park's transformation. *Mathematics and Computers in Simulation*, 38(4), 445–452.

Hamatwi, E., Davidson, I., Gitau, M., and Adam, G. (2016). Modeling and control of voltage source converters for grid integration of a wind turbine system. In *2016 IEEE PES PowerAfrica*, 98–106.

Hansen, A. and Michalke, G. (2009). Multipole permanent magnet synchronous generator wind turbines' grid support capability in uninterrupted operation during grid faults. *IET Renewable Power Generation*, 3(3), 333–348.

Haraguchi, H., Morimoto, S., and Sanada, M. (2009). Suitable design of a PMSG for a large-scale wind power generator. In *2009 IEEE Energy Conversion Congress and Exposition*, 2447–2452.

Heier, S. (2014). *Grid integration of wind energy: Onshore and offshore conversion systems*. John Wiley & Sons.

Kim, K., Jeung, Y., Lee, D., and Kim, H. (2012). LVRT scheme of PMSG wind power systems based on feedback linearization. *IEEE Transactions on Power Electronics*, 27(5), 2376–2384.

Kundur, P. (1994). *Power System Stability Analysis*. McGraw-Hill.

Mohseni, M. and Islam, S. (2012). Review of international grid codes for wind power integration: Diversity, technology and a case for global standard. *Renewable and Sustainable Energy Reviews*, 16(6), 3876–3890.

Muyeen, S., Takahashi, R., Murata, T., and Tamura, J. (2010). A variable speed wind turbine control strategy to meet wind farm grid code requirements. *IEEE Transactions on Power Systems*, 25(1), 331–340.

Tsili, M. and Papathanassiou, S. (2009). A review of grid code technical requirements for wind farms. *IET Renewable Power Generation*, 3(3), 308–332.

Uehara, A., Pratap, A., Goya, T., Senjyu, T., Yona, A., Urasaki, N., and Funabashi, T. (2011). A coordinated control method to smooth wind power fluctuations of a PMSG-based WECS. *IEEE Transactions on Energy Conversion*, 26(2), 550–558.

Van, T., Ngyen, T., Tran, T., and Nguyen, H. (2015). Advanced control strategy of back-to-back PWM converters in PMSG wind power system. *Advances in Electrical and Electronic Engineering*, 13(2), 81.

Xu, G., Xu, L., and Morrow, J. (2013). Power oscillation damping using wind turbines with energy storage systems. *IET Renewable Power Generation*, 7(5), 449–457.

Yassin, H., Hanafy, H., and Hallouda, M. (2016). Enhancement low-voltage ride through capability of permanent magnet synchronous generator-based wind turbines using interval type-2 fuzzy control. *IET Renewable Power Generation*, 10(3), 339–348.

Yuan, X. and Li, Y. (2014). Control of variable pitch and variable speed direct-drive wind turbines in weak grid systems with active power balance. *IET Renewable Power Generation*, 8(2), 119–131.

Yuan, X., Wang, F., Boroyevich, D., Li, Y., and Burgos, R. (2009). DC-link voltage control of a full power converter for wind generator operating in weak-grid systems. *IEEE Transactions on Power Electronics*, 24(9), 2178–2192.